Talanta 278 (2024) 126447

Contents lists available at ScienceDirect

Talanta

journal homepage: www.elsevier.com/locate/talanta

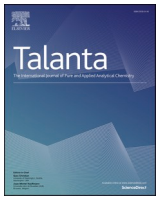

Development of a versatile optical pH sensor array for discrimination of anti-aging face creams

Cheng Cheng, Enzo Terreno *

Molecular & Preclinical Imaging Center, Department of Molecular Biotechnology and Health Sciences, University of Torino, 10126, Torino, Italy

ARTICLE INFO

Handling Editor: A Campiglia

Keywords:
Cosmetic products
pH sensor array
Fluorescence resonance energy transfer (FRET)
Anti-aging creams
Consumer health

ABSTRACT

The certification of cosmetic products has always been a prominent concern. Here, we have developed a pH sensor and applied it in the field of cosmetic safety. Initially, we designed two probes, CH with aggregation-induced emission (AIE) effect and the near-infrared fluorophore derivative CYTYR. By encapsulating them with DSPE-PEG2000-NH_2, we obtained the CHCY-lipo nano-micelles with fluorescence resonance energy transfer (FRET) response. By combining them into a sensor array called pC, we achieved sensitive detection of a wide pH range, ranging from 4.69 to 9.25. To validate the performance of the pC sensor array, we employed a multi-channel mode and applied it to differentiate commercial anti-aging creams. Through linear discriminant analysis and 3D fingerprint analysis, the pC sensor array successfully distinguished anti-aging creams from different countries, providing a rapid and accurate method for cosmetic safety identification. The results of this study demonstrate the potential of the pC sensor array for quick authentication of cosmetic products, offering significant support and application prospects in safeguarding consumer health.

1. Introduction

Anti-aging products are gaining popularity in the market [1]. Recently, with the increasing level of globalization, the phenomenon of counterfeit cosmetics has become more prevalent [2–4]. Profit-driven manufacturers produce and sell counterfeit and inferior products. One of the most common types of fraud is the adulteration of products claiming to be natural, often by adding cheaper ingredients and harmful chemicals (such as industrial-grade glycerin) along with other additives [5–9]. Another deceptive practice is counterfeiting and labeling low-quality, inexpensive anti-aging products with expensive brand names or producing the same product at different price points on the same production line. Combating cosmetic fraud is increasingly important.

The pH value plays a crucial role in cosmetics, especially in anti-aging creams, where it is considered an essential factor [10,11]. The pH value of a cream is crucial for its efficacy, stability, and compatibility with the skin. Anti-aging creams offer various benefits to humans, such as reducing wrinkles, increasing skin elasticity, and enhancing skin radiance, thereby keeping the skin youthful. These results are closely related to the pH environment of the cream. Typically, the pH range of anti-aging creams falls between 5 and 8, which is close to the natural acid-alkaline balance of the skin [12–14]. The correct pH value helps the active ingredients in the cream exert their optimal effects. For example, many anti-aging ingredients, such as antioxidants and peptides, are vital for maintaining the youthful state of the skin. However, these active ingredients remain stable within a specific pH range. Precisely controlling the pH of the cream ensures the stability of these active ingredients, providing the best anti-aging effects. Furthermore, the pH value of the cream also affects the compatibility with the skin. The pH value of the skin is typically maintained around 5.5, which is slightly acidic [15]. Creams that have a pH value similar to that of the skin are more easily absorbed and cause less irritation and discomfort. This is particularly important for individuals with sensitive skin. If the pH of the cream is too high or too low, it may damage the skin barrier, causing dryness, irritation, and discomfort. Therefore, ensuring an optimal pH value of anti-aging creams can maintain the skin in healthy condition and maximize the benefits of anti-aging products [1,7].

Fluorescent sensing arrays, often referred to as “artificial noses,” excel in substance identification. These sensors exhibit distinct luminescent characteristics when exposed to different substances, allowing for swift and accurate identification through linear discrimination. Their

* Corresponding author. Molecular & Preclinical Imaging Center, Department of Molecular Biotechnology and Health Sciences, University of Torino, Piazza Nizza 44bis, 10126, Torino, Italy.
E-mail address: enzo.terreno@unito.it (E. Terreno).

https://doi.org/10.1016/j.talanta.2024.126447
Received 20 March 2024; Received in revised form 12 June 2024; Accepted 17 June 2024
Available online 19 June 2024

applications span a broad spectrum, demonstrating remarkable proficiency in discerning drugs [16], explosives [17], and vapors within the realm of hazardous materials. In environmental applications, they effectively differentiate minerals [18] and organics in water resources [19]. In food safety, these arrays have successfully identified complex mixtures, including the nuanced aroma of coffee [20]. Notably, while fluorescent sensing arrays have found diverse applications, their utilization in evaluating skin care products remains an unexplored domain.

Over the past few decades, methods for identifying counterfeit cosmetics have been developed, including mass spectrometry, UV–vis spectroscopy, IR spectroscopy, and gas chromatography. [21–25] Although these techniques have been proven to be successful to some extent, certain drawbacks, such as expensive equipment and preliminary procedures for sample purification, hinder their widespread application in rapid identification [26–32]. Therefore, there is a need for the development of simple and rapid methods for discerning the authenticity and quality of cosmetics.

pH sensing arrays can simultaneously measure pH levels at various points in an environment. They offer excellent sensitivity, selectivity, and stability, and miniaturized and flexible designs for various applications. Recent advances include pH arrays using nanomaterials like graphene and carbon nanodots [33], but arrays for monitoring the pH of skin care products are less developed. The pH of an anti-aging face cream is crucial for its effectiveness and safety. Accurate pH measurement ensures that active ingredients remain stable and effective, maximizing the anti-aging benefits.

2. Results and discussion

This work aimed at designing a fluorescence pH sensing array, named pC, capable of detecting pH in a broad range of values and testing it on commercially available anti-aging face creams. The pC array consisted of three nanosized components CH-lipo CYTYR-lipo, and CHCY-lipo (A nanoparticle composed of a mixture of CH and CYTYR) based on CH and CYTYR dyes.

CH and CYTYR were synthesized through two simple synthetic steps (see Scheme 1).

CH molecule was obtained by the Knoevenagel condensation reaction of malononitrile-modified isoflurane and *p*-formylphenylboronic acid under argon protection, whereas CYTYR was synthesized with high yield by heating IR783 compound and tyramine in DMF. The choice of the two dyes was based on the expected pH dependence of their spectral properties.

Boronic acid moieties undergo deprotonation in alkaline solutions (pK_a 9–10), resulting in changes in their molecular properties, whereas malononitrile derivatives possess strong electron-withdrawing capabilities. On this basis, the connection between malononitrile and phenylboronic acid through a carbon-carbon double bond forms a large acceptor-acceptor (A-A) conjugated structure. However, under alkaline conditions, boronic acid undergoes deprotonation, and the molecular structure transforms into a donor-acceptor (D-A) system, leading to significant spectral changes. Although CH dye has been already reported in literatures, it has never been investigated as pH sensor [34].

The CYTYR dye was selected for the peculiar pH dependence of its spectral pattern, which is the result of the protonation of the meso-amino group, whose pK_a was reported to be in the 3–6 range [35], thus extending the pH detection range of the array to the acidic side. Additionally, the spectral properties of CH and CYTYR are ideal for promoting a FRET system, with CH as the donor and CYTYR as the acceptor.

To enable FRET mechanism and overcome the low water solubility of the dyes, CH and CYTYR were formulated, individually and in combination, with 1,2-distearoyl-*sn*-glycero-3-phosphoethanolamine (DSPE-PEG2000-NH2) to form nanomicelles in water [36–41], which also improves the stability of the pC array. The absorption and fluorescence properties of CH-lipo, CYTYR-lipo, and CHCY-lipo can exhibit different and distinct pH profiles, and their combination enables a wide range of pH detection and discrimination. The tyrosine-modified cyanine dye CYTYR was considered as the energy acceptor. At low pH values, CH dye exhibits weak fluorescence, and its emission wavelength does not match the absorption of CYTYR, resulting in no FRET effect. However, when pH increases, CH undergoes deprotonation, resulting in a red shifted emission and FRET coupling with the CYTYR acceptor. Therefore, the combination of these dyes' spectral features may extend the pH sensing

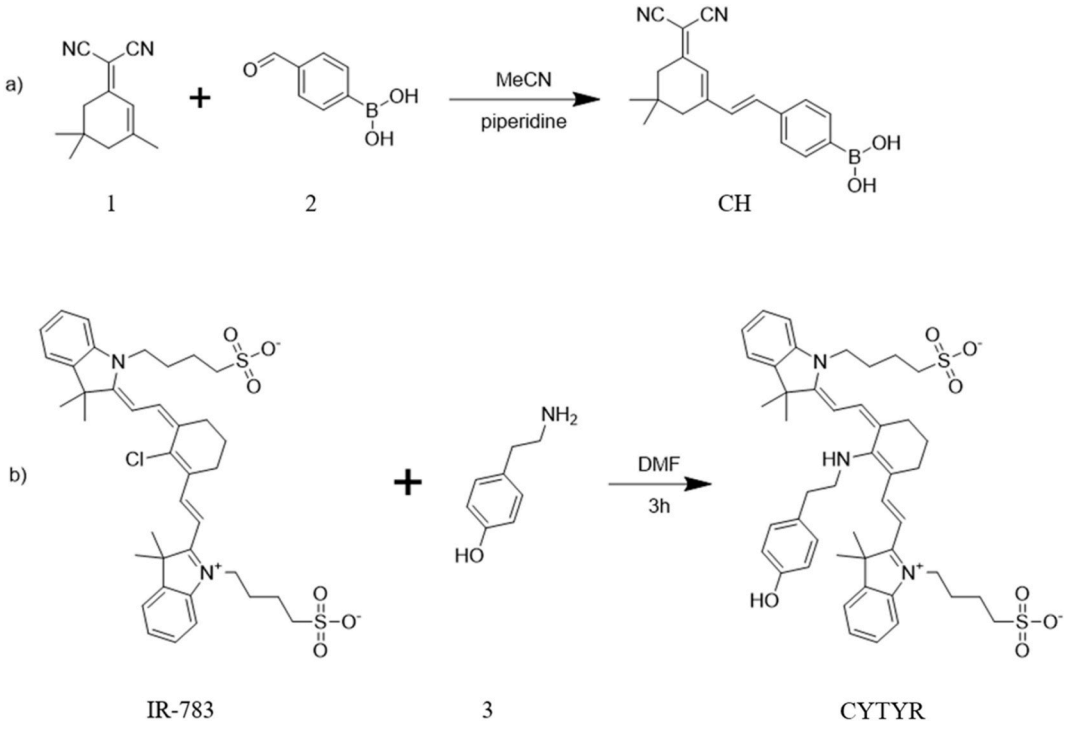

Scheme 1. Synthetic routes of CH (a) and CYTYR (b).

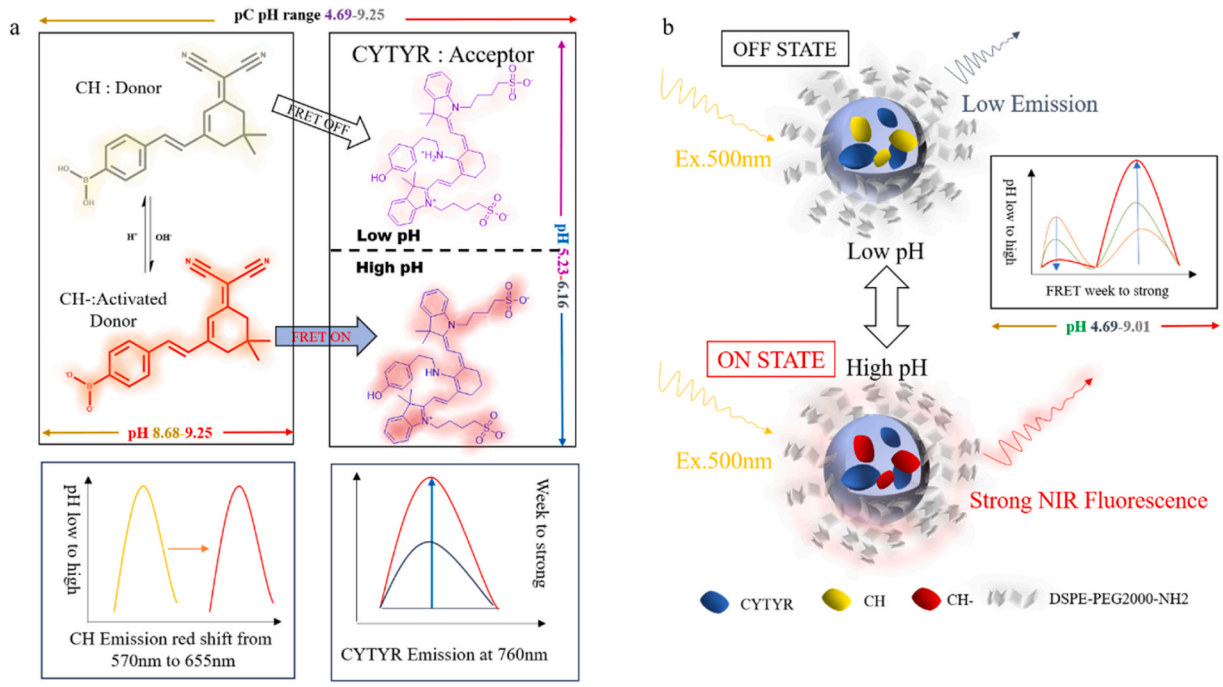

Scheme 2. a) Chemical structures of the pre-donor CH, donor CH-, and pH-activated acceptor CYTYR. b) Illustration of the pH response of CHCY.

range across both acidic and alkaline regions, in the 4.7–9.2 range (Scheme 2).

First, the spectral characteristics of CH and CYTYR dyes were evaluated in THF and methanol, respectively (Fig. S1). The maximum absorption and emission wavelengths pairs were 400/490 nm for CH, and 645/760 nm for CYTYR.

Interestingly, under alkaline conditions (pH 11), CH deprotonated with a consequent red shift of the absorption/emission pair and increase of the Stokes shift (450 nm/650 nm). Interestingly, in this condition the emission wavelength of the deprotonated CH dye matched well the absorption of CYTYR dye, thus enabling an energy transfer (Scheme 2a, Fig. S2). CH and CYTYR dyes also exhibited a solvent-dependent fluorescence (Fig. S3). Compared to THF, the emission of CH was reduced in hexane (associated with a blue shift), in methanol and DMF (associated with a red shift in both solvents) and increased in acetonitrile and chloroform. Compared to methanol, the fluorescence intensity of CYTYR was reduced in acetonitrile (blue shift) and chloroform (no shift) and was similar in DMF. All these observations are in good agreement with the solubility of the dyes in the different solvents and the effect of solvent polarity on the spectral pattern.

The concentration dependence of the fluorescence emission was determined for both the dyes. The emission of CH in THF showed a linear behavior up to a concentration around 10 μM, after which the fluorescence quenched and decreased for a concentration higher than 50 μM, likely due to collisional quenching effects (Fig. S4). Also the concentration dependence for CYTYR in methanol exhibited a linear correlation up to 10 μM, and a limited quenching at higher concentrations (Fig. S5).

It is worth noting that upon addition of water in a 10 μM THF solution of CH, the typical pattern resulting from the occurrence of aggregation-induced emission (AIE) effects. In fact, upon increasing the water fraction, the emission of the dye at 500 nm progressively decreased with a consequent appearance of a redshift emission at 570 nm, which is the only emission detectable when the water fraction reached 98 % (Fig. S6a). Plotting the fluorescence intensity 570/500 ratio, a steep increase of the red shift emission due to the AIE effect was detected water content larger than 70 % (Fig. S6b).

To overcome the dyes' limited water solubility and promote a pH-dependent FRET mechanism, the CH/CYTYR pair was formulated into nanoaggregates using DSPE-PEG2000-NH2 phospholipid (7.5 mol%) as a surfactant (CHCY-lipo). Formulations containing the individual dyes CH (CH-lipo) and CYTYR (CYTYR-lipo) were also prepared.

The nanoparticle features of the formulations were evaluated by Dynamic Light Scattering measurements, which allowed the determination of the average hydrodynamic size, polydispersion index, and the zeta-potential of the aggregates at pH 4.4, 7.4, and 11.6 (Table S1). The aggregates spanned a quite broad size range, from 90 nm to 600 nm, and size dispersion (0.05–0.5), without a clear dependence on pH and dye composition. As expected, the zeta-potential generally displayed high negative values at pH 11.6, and more positive values as pH decreased, likely reflecting the deprotonation of the terminal amino group of the phospholipid used in the formulation.

The mixed CHCY-lipo sample was also formulated as a function of the CH/CYTYR molar ratio from 1:1 to 1:10. The emission spectra of these samples (excitation at 500 nm) at pH 11.6 are displayed in Fig. S7. FRET effect started to be detectable in the formulation with the 1:4 M ratio and reached the maximum efficiency (E = 96.4 %) for the 1:10 formulation.

The FRET process is promoted by the incorporation of the dyes in the nanoaggregates and upon addition of TritonX-100 for disassembling the nanoparticles, the emission of the CH dye was recovered (Fig. S8).

Next, the spectral properties and pH responsiveness of CH-lipo, CYTYR-lipo, and CHCY-lipo was assessed.

The absorption spectra of CH-lipo over the 2–10 pH range displayed a pattern fully consistent with the presence of an acid-base equilibrium with a maximum absorption around 410 nm at acidic pH and a broader red shifted signal around 500 nm at the basic side (Fig. 1a). By plotting the pH dependence of the absorption 500/410 nm ratio, a clear inflection point at *ca.* pH 9 was observed, in agreement with the expected pK_a for a phenylboronic moiety (Fig. S9a).

The fluorescence emission of CH-lipo (excitation at 500 nm) reflected the absorption pattern, with a signal at 570 nm for the protonated dye, and a red shifted emission at 655 nm for the deprotonated molecule (Fig. 1b). The values of the fluorescence intensity 655/570 ratio were fitted with an S-shaped Boltzmann function, and a pK_a values of 8.96 (in good agreement with the deprotonation of the phenylboronic

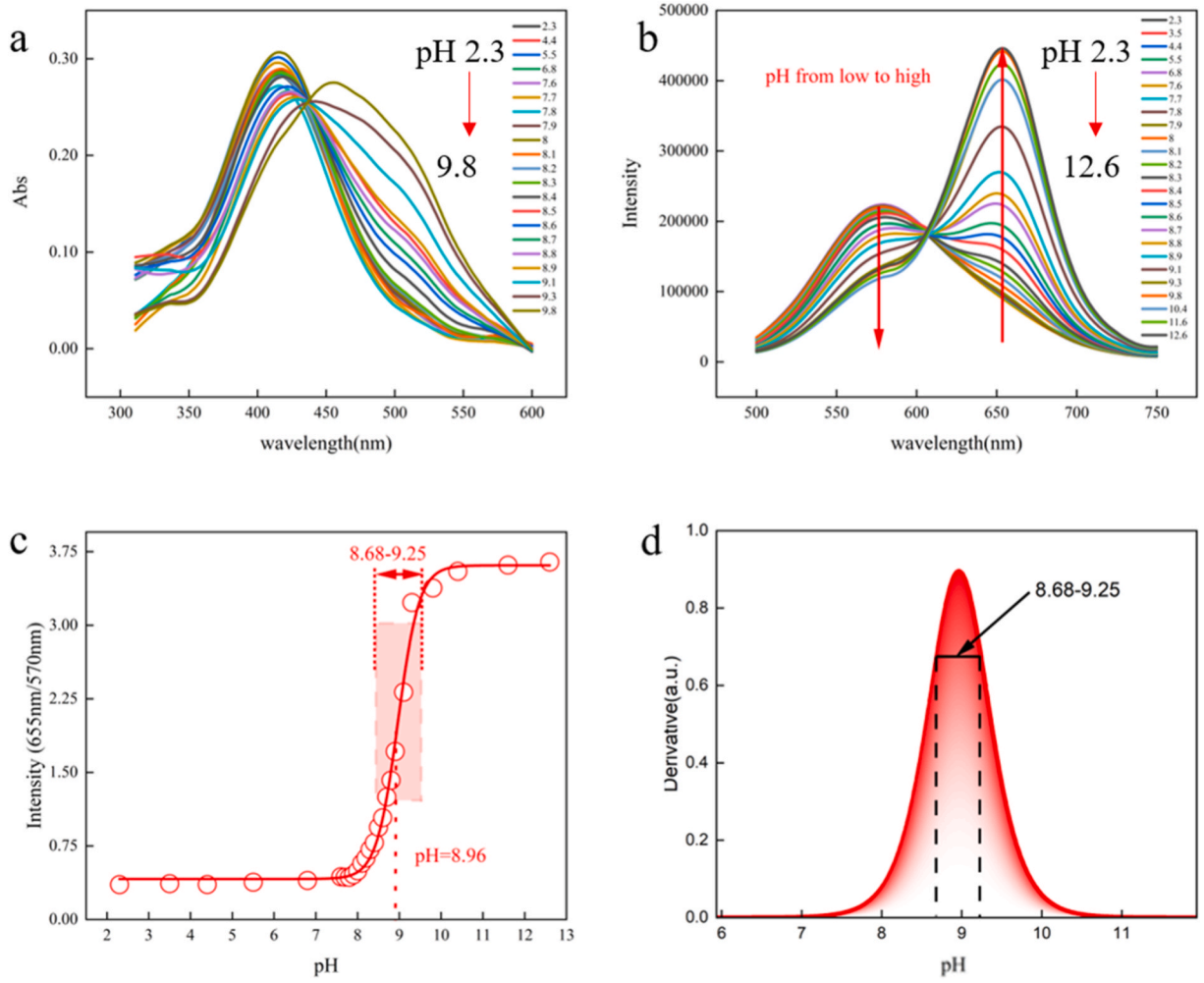

Fig. 1. a) UV absorption spectra of CH-lipo in different pH buffer solutions. b) Fluorescence emission spectra of **CH-lipo** in different pH buffer solutions at a concentration of 20 μM. Excitation wavelength: 500 nm, slit width: 3 nm. c) Sigmoidal Boltzmann function fitting curve of the ratio of fluorescence intensities at 655 nm and 570 nm as a function of pH. d) Derivative curve of the fitting function in Fig. 1c, where 75 % of the maximum value is taken as the pH-sensitive response range.

acid moiety) was obtained from the inflection point (Fig. 1c). A pH detection range between 8.68 and 9.25 (ΔpH = 0.57) was determined for this system (Fig. 1d, Figs. S9b–c).

CYTYR-lipo sample exhibited a different behavior. In acidic environment, the dye displayed an absorption peak around 500 nm, whose intensity decreased under alkalization, while a red shifted absorption around 630 nm appeared and reached the maximum intensity at pH 7.8. The blue shifted absorption in acidic condition can attributed to the protonation of the amino group located at the *meso* position of the polymethine chain of the dye as already reported for other similar systems [35,42]. Therefore, in neutral and alkaline conditions, the meso-amino group deprotonates, and the absorption spectrum displays the typical pattern associated with a cyanine dye (Fig. 2a). Similarly, the fluorescence emission (excitation at 645 nm) displayed a pH dependence in excellent agreement with the presence of acid/base pair with a pK_a of 5.7 (Fig. 2b–d). Consequently, the pH detection range of this system was found to be 5.23–6.16 (ΔpH = 0.93).

The spectral pattern of the mixed formulation CHCY-lipo (CH/CYTYR 1:10 M ratio) is shown in Fig. 3.

The absorption spectra showed a complex pattern in the 400–500 nm range, with a general reduction in signal intensity from acidic to alkaline environments and an opposite trend in the 600 nm region. Alkaline conditions produced a new absorption peak at 450–500 nm (Fig. 3a). The emissive pattern of this sample (upon excitation at 500 nm) was predominantly characterized by a single emission at 760 nm arising from the CYTYR dye, whose intensity progressively increased over the 3–12 pH interval (Fig. 3b–c).

The combined effect of CYTYR and CH deprotonation and the resulting FRET effect in the nanoaggregates, upon excitation at 500 nm, extended the pH responsiveness of this system over more than 4 pH units (4.69–9.01).

With the aim of assessing the potential of the nanoaggregates for pH sensing purposes of anti-aging creams, their photostability and possible interferences with metal ions were evaluated.

CH-lipo exhibited excellent photostability during multiple acid-base cycles (pH 3.4 and 12.6), while CYTYR-lipo and CHCY-lipo showed a slight reduction in the fluorescence emission in the same challenge (Figs. S11a–c).

Concerning potential interference with the presence of metal ions, the results reported in Fig. S11d demonstrate that the emission of the three systems is almost unaffected by the presence of nine metal ions selected for this experiment.

Based on these promising observations and the distinct pH sensing properties of CH-lipo, CYTYR-lipo, and CHCY-lipo, we established the pC pH sensing array (Scheme 3).

The sensing array was conceived with six channels utilizing the UV–vis absorption and fluorescence emission of CH-lipo, CYTYR-lipo, and CHCY-lipo for detection. Each probe was mixed with buffers at

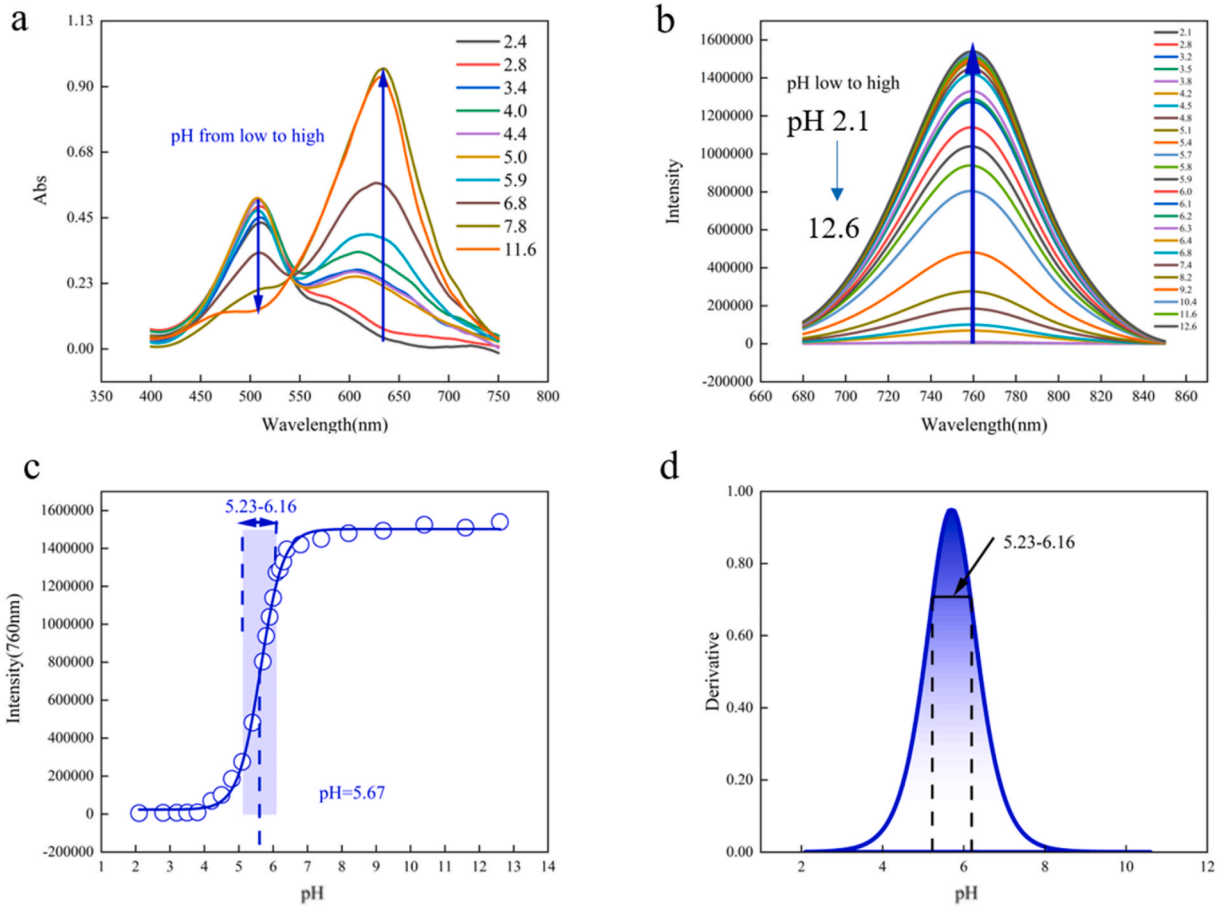

Fig. 2. a) UV absorption spectra of CYTYR in different pH buffer solutions. b) Fluorescence emission spectra of CYTYR-lipo in different pH buffer solutions at a concentration of 20 μM. Excitation wavelength: 645 nm, slit width: 3 nm. c) Sigmoidal Boltzmann function fitting curve of the ratio of fluorescence intensities at 760 nm as a function of pH. d) Derivative curve of the fitting function in Fig. 2c, where 75 % of the maximum value is taken as the pH-sensitive response range.

different pH values, and the final concentration of dyes was set to 20 μM. The absorption and fluorescence intensities were recorded after 3 min. As shown in Fig. 4a, pC array exhibited different quenching effects at the different examined pH values. The quenching ratio (calculated as $(I–I_0)/I_0$ or $(A - A_0)/A_0$) for all sensing channels were measured within the range of −1 to 1.5, with pH 7.4 in PBS solution as reference. Linear discriminant analysis (LDA) was used to generate a fingerprint pattern for the pH sensing of the array (Fig. 4b). The first two principal components (83.2 % and 15.3 %) were sufficient to easily differentiate the pH values, as better highlighted in the 3D fingerprint pattern (Fig. 4c).

Then, we applied the pC array to test a series of eight popular anti-aging worldwide produced face creams available in the market. High-quality products often use natural ingredients to protect the skin, while counterfeit products may add chemicals to achieve a deceptive appearance, leading to irreversible damage with long-term use. For example, polyphenols can act as antioxidants in skin care products.

However, polyphenolic compounds, particularly flavonoids, can interact with proteins through nonspecific forces (e.g., hydrogen bonding and hydrophobic effects) and covalent bond formation, forming complexes that impact protein function, solubility, and stability [43]. Some unscrupulous manufacturers achieve this effect by adding phenol, but excessive phenol can cause skin discomfort. Excess phenol can affect the pH of skin care products, and we can use pC to identify it. The declared pH values of the anti-aging face creams ranged between 5.4 and 8.1 (Table S2). Solution of face cream at a concentration of 10 mg/mL was mixed with the pC array, resulting in a final dye concentration of 20 μM, and absorbance and emission were measured in the six channels (Fig. 5). Different quenching ratios were measured for each channel for the various creams. Face creams 1 and 2 exhibited significant quenching, while creams 5 and 6 showed similar quenching patterns. The 2D fingerprint pattern successfully separated six of the face creams, but it was unable to differentiate face creams 4 and 7 as well as 6 and 8, which showed some overlapping (Fig. 5b). By incorporating a third factor in the LDA analysis (Factor 1: 74.2 %, Factor 2: 23.7 %, Factor 3: 1.7 %), and analyzing the 3D spatial fingerprint pattern, all the creams were well differentiated (Fig. 5c).

We further challenged the pC array with a solution of two randomized cream mixtures at a concentration of 10 mg/mL. The results indicated that pC performed well in the test. The two-dimensional fingerprint pattern successfully separated multiple blends of creams, with only individual overlaps when Cream 1 and Cream 3 were mixed with the other creams (Fig. S12). However, by adding a third factor, the three-dimensional spatial fingerprint pattern successfully analyzed all mixture solutions, with each mixture of creams having its own unique fingerprint pattern, suggesting that pC array has also a great potential for mixture identification (Fig. S13).

To further validate the accuracy of the pC array, we randomly selected a supplementary package of one face cream as an unknown sample for testing, and the results showed that the method successfully identified Cream X as the supplementary package of Cream 7 (Fig. 6a). In the ongoing exploration of the discriminative performance of pC array against counterfeit creams, we intentionally introduced various substances (formaldehyde, phenol, mercury ions, hydrogen peroxide, and acetone) into the selected eight creams. These substances are common industrial compounds used in producing fraudulent cosmetics. The 3D fingerprint of cream 1 added with the “counterfeiting” substances

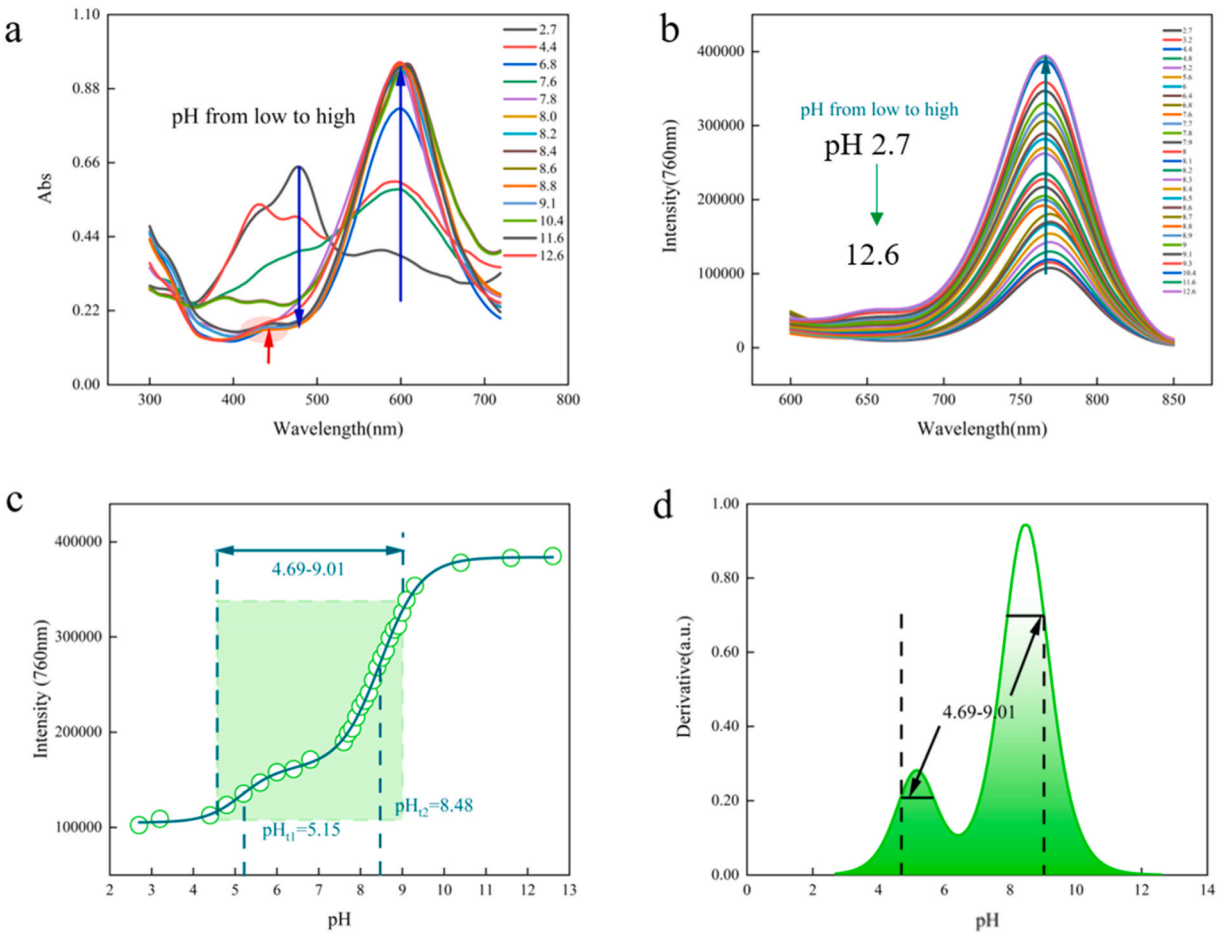

Fig. 3. a) UV absorption spectra of CHCY in different pH buffer solutions. b) Fluorescence emission spectra of CHCY-lipo in different pH buffer solutions at a concentration of 20 μM. Excitation wavelength: 500 nm, slit width: 3 nm. c) Sigmoidal double Boltzmann function fitting curve of the ratio of fluorescence intensities at 760 nm as a function of pH. d) Derivative curve of the fitting function in Fig. 3c, where 75 % of the maximum value is taken as the pH-sensitive response range.

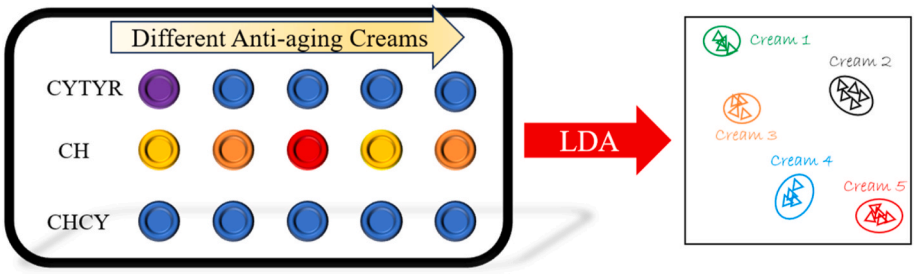

Scheme 3. Explanation of the application of the pC sensor array in differentiating various anti-aging creams.

revealed a distinct identification of the modified cream (Fig. 6b), likely attributable to pH alterations and/or changes in the physico-chemical properties of the dyes induced by the added substances. Encouragingly, analogous positive outcomes were achieved for the remaining creams as well (Fig. S14). Notably, the entire identification process for each set of samples was completed within 15 min, demonstrating the rapid, accurate, and convenient characteristics of the test.

Compared to conventional pH testing, this study offers the advantages of speed and accuracy. However, it also has certain limitations. The number of samples used in this study is relatively small, especially when considering the vastness of the cosmetics market. Future research could leverage machine learning techniques to expand the trial range of the array. Machine learning can effectively reduce time costs and accelerate the commercialization of the array.

3. Conclusions

In summary, this work reports the synthesis and characterization of two novel dyes, CH and CYTYR, with peculiar pH responsiveness properties. CH exhibits aggregation-induced emission (AIE) effect in water and undergoes a red shifted fluorescence emission under alkaline conditions that matches the absorption of CYTYR, thus allowing an efficient FRET effect. The dyes were combined with a phospholipid to form nanoaggregates, whose spectral patterns were utilized to design a six-channel pH sensing array with a pH detection interval between 4.7 and 9.25. The performance of this array was tested to evaluate the quality of eight commercially available anti-aging face creams. Linear discriminant analysis of the 3D fingerprint patterns demonstrated the ability of the array to effectively distinguish the different brands of the

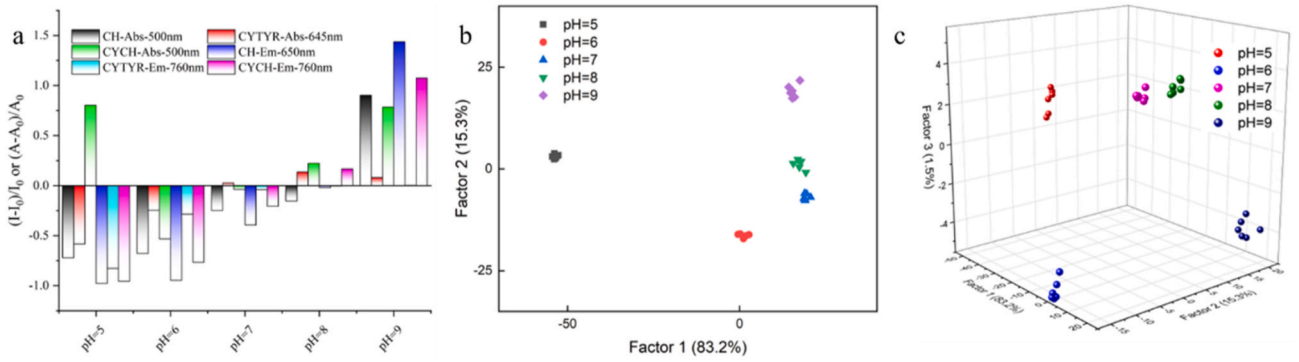

Fig. 4. a) Quenching ratios of pC at different pH values. b) Two-factor linear discriminant analysis fingerprint plot of pC for pH sensing. c) Three-factor linear discriminant analysis spatial fingerprint plot of pC for pH sensing.

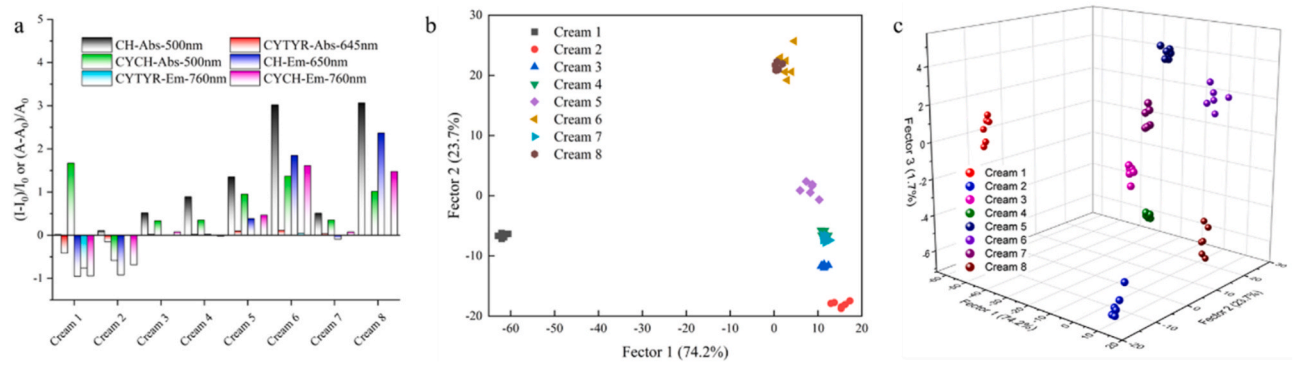

Fig. 5. a) Quenching ratios of pC at different creams. b) 2D analytical fingerprints of pC with eight face creams. c) Three-factor linear discriminant analysis spatial fingerprint plot of pC for creams sensing.

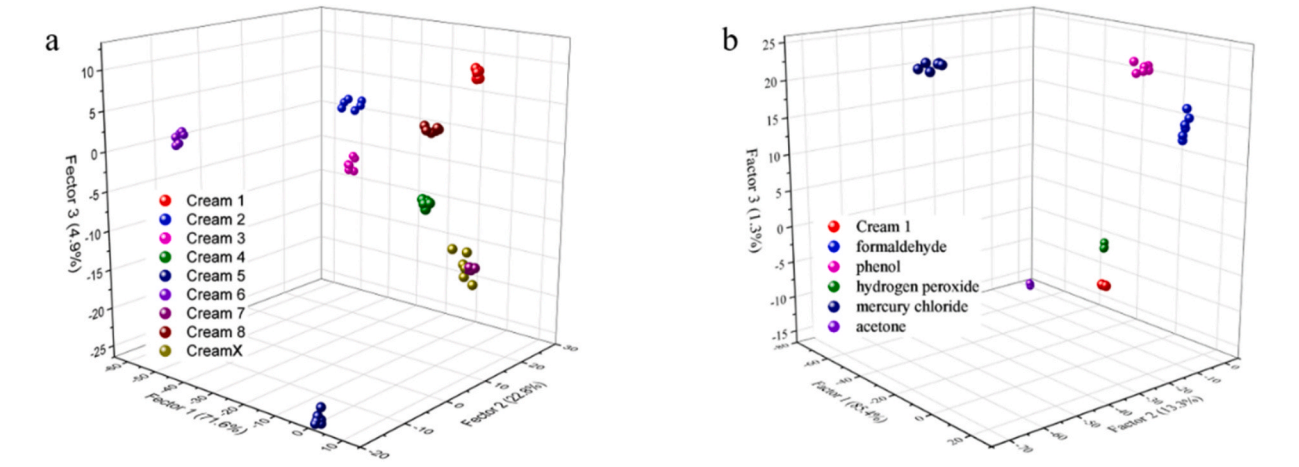

Fig. 6. a) 3D fingerprinting of unknown cream X identified by pC. b) 3D fingerprinting of cream 1 with **pC** identification of added and unadded industrial compounds.

anti-aging products. Moreover, the array was challenged to analyze artificially sophisticated creams, further confirming the great potential to assess the quality of the products and identify possible frauds. The characterization of the products was completed within 15 min, showcasing the potential of the method in quality control tests in cosmetics industry.

4. Experimental section

4.1. Materials and methods

Unless otherwise specified, materials were obtained from Sigma-Aldrich and used without further purification. DSPE-PEG2000-NH2 (25 mg/mL in chloroform solution) was purchased from Sigma. Deionized water was obtained by Milli-Q water purification system (Millipore) with electrical conductivity of 18.2 s/m. Using tetramethylsilane (TMS) as the internal standard, 1H and 13C NMR spectra were recorded on 14 T

Bruker Avance III spectrometer. Mass spectra were recorded on the Brook Electron spray Ionization Mass Spectrometer (ESI-MS). The UV–Vis absorption spectrum was collected by CARY50 biological spectrophotometer (Varian Inc., CA., USA). Fluorescence spectra were measured on Fluoromax-4 fluorescence spectrophotometer (HoribaJobinYvon Inc., USA). Spectra were recorded at 25 °C, with excitation and emission slits of 3 nm. The 8 anti-aging creams used in this study were unopened samples provided by the manufacturers at the time of purchase. All samples were within their expiration dates, ensuring their freshness and effectiveness.

4.2. Synthesis of CH

Compound CH was synthesized using a method described in previously published literature [40]. Under argon gas protection, compound **1,** 2-(3,5,5-trimethylcyclohex-2-en-1-ylidene)malononitrile (0.2 g, 1.07 mmol) and 4-hydroxybenzaldehyde (**2**, 0.22 g, 1.5 mmol) were dissolved in 3 mL acetonitrile. Then piperidine (0.5 mL, 5.06 mmol) was added to the solution and the mixture was heated to reflux at 85 °C for 16 h. The reaction was monitored until reactant **1** disappeared. Subsequently, the solution was extracted using ethyl acetate (3 × 25 mL) and water. The organic layer was washed with 1 N HCl (30 mL) and saturated salt water, before being dried with anhydrous sodium sulfate to obtain red crude solid. Column chromatography separation (dichloromethane: methanol = 60:1 to 10:1) resulted in 162 mg (orange solid) with a yield of 51 %.^{1}H NMR (600 MHz, DMSO-d_6) δ 8.10 (s, 2H), 7.81 (d, J = 7.6 Hz, 2H), 7.66 (d, J = 7.7 Hz, 2H), 7.47 (d, J = 16.1 Hz, 1H), 7.28 (d, J = 16.2 Hz, 1H), 6.92 (s, 1H), 2.63 (s, 2H), 2.56 (s, 2H), 1.01 (s, 6H)., ^{13}C NMR (151 MHz, DMSO) δ 170.96, 156.33, 138.08, 137.96, 135.16, 130.59, 127.37, 123.63, 114.42, 113.59, 77.15, 42.91, 40.65, 40.53, 40.39, 40.26, 40.12, 39.98, 39.84, 39.70, 38.74, 32.27, 28.02, 27.65. MS (ESI): calculated for $C_{19}H_{19}BN_2O_2$ $[M+H]^+$: 318.15, found 318.15.

4.3. Synthesis of CYTYR

CYTYR was synthesized in a one-step reaction from IR783(2-[2-[2-Chloro-3-[2-[1,3-dihydro-3,3-dimethyl-1-(4-sulfobutyl)-2H-indol-2-ylidene]-ethylidene]-1-cyclohexen-1-yl]-ethenyl]-3,3-dimethyl-1-(4-sulfobutyl)-3H-indolium hydroxide). IR783 and tyramine (**3)** were dissolved in 1 mL of DMF and reacted at 85 °C for 3 h. The solvent was then removed by vacuum distillation. Column chromatography separation (dichloromethane: methanol = 3:1 to 1:1) resulted in 36 mg blue solid with a yield of 61 %.^{1}H NMR (600 MHz, Methanol-d4) δ 8.00 (s, 1H), 7.68–7.63 (m, 1H), 7.35 (d, J = 7.4 Hz,2H), 7.31 (t, J = 7.9 Hz, 2H), 7.08 (t, J = 3.5 Hz, 8H), 6.78 (dd, J = 16.2, 8.0 Hz, 4H), 3.98 (d, J = 6.8 Hz, 4H), 3.02 (s, 4H), 2.89 (q, J = 7.3 Hz, 6H), 2.51 (t, J = 6.5 Hz, 3H), 1.94 (s, 8H), 1.61 (s, 12H).^{13}C NMR (151 MHz, MeOD) δ 169.85, 165.81, 158.33, 145.46, 142.23, 140.38, 133.33, 132.20, 131.72, 131.65, 130.79, 130.55, 130.34, 129.29, 124.77, 123.91, 122.80, 117.67, 117.62, 111.07, 96.71, 70.05, 53.24, 52.99, 44.68, 43.17, 41.12, 38.17, 37.87, 34.72, 32.56, 31.06, 30.03, 27.68, 27.10, 25.89, 25.56, 24.94, 24.60, 23.55, 15.31, 12.32. MS (ESI): calculated for $C_{46}H_{56}N_3O_7S_2^-$ $[M+H]^+$: 826.36, found 826.19.

4.4. Preparation of phospholipid-based sensors

CH-lipo and CYTYR-lipo sensors were prepared using the modified film hydration technique. Initially, CH was dissolved in THF and CYTYR was dissolved in methanol to create a stock solution with a concentration of 1 mM for both chemicals. A mixture of 0.01 mL CH or CYTYR (10 μmol) from the stock solution and 0.03 mL of DSPE-PEG2000-NH_2 (25 mg/mL in $CHCl_3$) was prepared at a mass ratio of approximately 1:100. The organic solvent was then removed using vacuum rotary evaporation, resulting in a dry lipid film containing the dye. The dried film was hydrated with 1 mL of deionized water and sonicated for 1 min to obtain a clear stock solution of the two sensors with a dye concentration of 20 μM, which was used for absorbance and emission measurements.

For the CHCY-lipo sensor, the following general methods were employed. CH and CYTYR stock solutions were mixed at a molar ratio of 1:10 (10 μL CH 1 mM in THF + 100 μL CYTYR 1 mM in MeOH) and combined with DSPE-PEG2000-NH_2 (25 mg/mL in $CHCl_3$) at a mass ratio of approximately 1:15. The organic solvent was then removed by vacuum rotary evaporation, resulting in a dry lipid film containing the dyes. The dried film was hydrated with 1 mL of deionized water and subjected to sonication for 1 min to obtain a clear stock solution of sensors with a CH/CYTYR dye concentrations of 10 μM/100 μM. To prepare the test sensors solution, 0.2 mL of the stock sensors solution was mixed with different pH buffers (0.8 mL), resulting in a test sensors solution with a CH/CYTYR dye concentrations of 2 μM/20 μM for absorbance and emission measurements. Other CHCY-lipo sensors were prepared differing in the CH/CYTYR molar ratios: 1:1, 1:4, 1:6 and 1:8.

4.5. FRET efficiency

The efficiency of FRET effect (E) was calculated according to the following equation: $E = 1 - (F_{DA}/F_D)$ S1

where FDA is the fluorescence intensity of the donor (CH) in the presence of the acceptor (CYTYR), and FD is the fluorescence intensity of the donor in the absence of the acceptor.

4.6. Assessment of pH responsiveness of the sensors

Using CH as a typical example, the probes were incubated with various ionic solutions at a concentration of 10 mM. The fluorescence spectra were measured to evaluate the response reliability. The $ONOO^-$ was prepared using the method described in the published literature [44].

A buffer solution (10 mM) was prepared by dissolving citric acid and sodium citrate in water to test a broad pH range from 2.0 to 11.0. CH-lipo, CYTYR-lipo, and CHCY-lipo were added to the appropriate pH buffer solutions to obtain a concentration of fluorescent dyes of 20 μM. Fluorescence readout were recorded using a Microplate reader using the following excitation and emission wavelengths:

CH-lipo: Excitation at 500 nm, Emission at 650 nm.
CYTYR-lipo: Excitation at 645 nm, Emission at 760 nm.
CHCY-lipo: Excitation at 500 nm, Emission at 760 nm.

4.7. pC to distinguish anti-aging creams

To obtain a 1 mg/mL solution, the 8 investigated face creams were dispersed in water. The resulting solutions were then distributed evenly in a 96-well plate in a 8x3 arrangement. Next, the pH sensors were added to the wells, obtaining a solution with a concentration of 20 μM of fluorescent material. The plate was carefully handled to ensure proper mixing of the sensor with the face cream solution in each well. The plate was then placed in a microplate reader equipped with UV fluorescence detection capabilities. The reader was set to record the UV fluorescence data at the appropriate excitation and emission wavelengths for the sensors used. The test for the unknown cream was carried out similarly to the experiment above. The parameters of the six detection channels are:

Channel 1 and Channel 2 are for CH-lipo, Excitation at 500 nm, Emission at 650 nm.

Channel 3 and Channel 4 are for CYTYR-lipo, Excitation at 645 nm, Emission at 760 nm.

Channel 5 and Channel 6 are for CHCY-lipo, Excitation at 500 nm, Emission at 760 nm.

Notes

The authors declare no competing financial interest.

CRediT authorship contribution statement

Cheng Cheng: Writing – review & editing, Writing – original draft, Validation, Methodology, Investigation, Formal analysis, Data curation, Conceptualization. **Enzo Terreno:** Writing – review & editing, Supervision, Resources, Project administration, Funding acquisition, Formal analysis, Data curation, Conceptualization.

Declaration of competing interest

The authors declare that they have no known competing financial interests or personal relationships that could have appeared to influence the work reported in this paper.

Data availability

No data was used for the research described in the article.

Appendix A. Supplementary data

Supplementary data to this article can be found online at https://doi.org/10.1016/j.talanta.2024.126447.

References

[1] A. Muise, S. Desmarais, Women's perceptions and use of "anti-aging" products, Sex. Roles 63 (2010) 126–137.
[2] M.S. Ferreira, M.C. Magalhaes, J.M. Sousa-Lobo, I.F. Almeida, Trending anti-aging peptides, Cosmetics 7 (4) (2020) 91.
[3] A.N. Zaid, R. Al Ramahi, Depigmentation and anti-aging treatment by natural molecules, Curr. Pharm. Des. 25 (20) (2019) 2292–2312.
[4] N. Chondrogianni, S. Kapeta, I. Chinou, K. Vassilatou, I. Papassideri, E.S. Gonos, Anti-ageing and rejuvenating effects of quercetin, Exp. Gerontol. 45 (10) (2010) 763–771.
[5] R.H. Binstock, The war on "anti-aging medicine", Gerontol. 43 (1) (2003) 4–14.
[6] S. Baydanoff, E. Konova, N. Ivanova, Determination of anti-AGE antibodies in human serum, Glycoconj. J. 13 (3) (1996) 335–339.
[7] A. Muise, S. Desmarais, Women's perceptions and use of "Anti-Aging" products, Sex. Roles 63 (1–2) (2010) 126–137.
[8] C.E. Mykytyn, Anti-aging medicine: a patient/practitioner movement to redefine aging, Soc. Sci. Med. 62 (3) (2006) 643–653.
[9] I. Mevlitoglu, B. Engin, M. Kaplan, How effective are anti-ageing products? Turkderm-Turkish Archives of Dermatology and Venerology 43 (2009) 2–6.
[10] I. Nesic, V. Savic, A. Kolarevic, Investigation of efficacy of anti-aging liposomal intimate gel: an in vivo long-term study, Acta Fac. Med. Naissensis 37 (1) (2020) 48–56.
[11] C.C. Felippi, D. Oliveira, A. Stroher, A.R. Carvalho, E. Van Etten, M. Bruschi, R. P. Raffin, Safety and efficacy of antioxidants-loaded nanoparticles for an anti-aging application, J. Biomed. Nanotechnol. 8 (2) (2012) 316–321.
[12] B. Eren, S.T. Tanriverdi, F.A. Kose, O. Ozer, Antioxidant properties evaluation of topical astaxanthin formulations as anti-aging products, J. Cosmet. Dermatol. 18 (1) (2019) 242–250.
[13] T.R. Chang, H. Li, H.N. Lv, M.H. Tan, S.B. Hou, X. Liu, M. Lian, Q.S. Zhao, B. Zhao, Extraction, physicochemical properties, anti-aging, and antioxidant activities of polysaccharides from industrial hemp residues, Molecules 27 (18) (2022) 5746.
[14] G.P. Hong, S.G. Min, Y.J. Jo, Anti-oxidative and anti-aging activities of porcine by-product collagen hydrolysates produced by commercial proteases: effect of hydrolysis and ultrafiltration, Molecules 24 (6) (2019) 1104.
[15] S.M. Ali, G. Yosipovitch, Skin pH: from basic science to basic skin care, Acta Derm. Venereol. 93 (3) (2013) 261–267.
[16] S. Eissa, R.A. Almthen, M. Zourob, Disposable electrochemical immunosensor array for the multiplexed detection of the drug metabolites morphine, tetrahydrocannabinol and benzoylecgonine, Microchim. Acta 186 (2019) 1–9.
[17] C. Cheng, L. Chao-Yi, S.-A. Shahzad, Z. Hui-Peng, Y. Cong, J. Xing, Phenothiazine and BN-doped AIE probes integrated fluorescence sensor array for detection and discrimination of nitro explosives, Chin. J. Anal. Chem. 48 (7) (2020) e20075–e20080.
[18] Y. Li, J. Hou, H. Zhou, M. Jia, S. Chen, H. Huang, L. Zhang, C. Yu, A fluorescence sensor array based on perylene probe monomer-excimer emission transition for the highly efficient differential sensing of metal ions and drinking waters, Sens. Actuators, B 319 (2020) 128212.
[19] C. Zhang, K.S. Suslick, A colorimetric sensor array for organics in water, J. Am. Chem. Soc. 127 (33) (2005) 11548–11549.
[20] B.A. Suslick, L. Feng, K.S. Suslick, Discrimination of complex mixtures by a colorimetric sensor array: coffee aromas, Anal. Chem. 82 (5) (2010) 2067–2073.
[21] J.A.R. Teodoro, H.V. Pereira, D.N. Correia, M.M. Sena, E. Piccin, R. Augusti, Forensic discrimination between authentic and counterfeit perfumes using paper spray mass spectrometry and multivariate supervised classification, Anal. Methods 9 (34) (2017) 4979–4987.
[22] L.N. Al-Eitan, H.A. Aljamal, R.Q. Alkhatib, Gas chromatographic-mass spectrometric analysis of sunscreens and their effects on mice liver and kidney enzyme function, Clin. Cosmet. Invest. Dermatol. 12 (2019) 11–21.
[23] N.J. Sadgrove, Honest nutraceuticals, cosmetics, therapies, and foods (NCTFs): standardization and safety of natural products, Crit. Rev. Food Sci. Nutr. 62 (16) (2022) 4326–4341.
[24] M. Malet-Martino, R. Martino, Analysis of counterfeit medicines and adulterated dietary supplements by NMR, Emagres 4 (1) (2015) 159–170.
[25] S. Paraschos, P. Magiatis, E. Gikas, I. Smyrnioudis, A.L. Skaltsounis, Quality profile determination of Chios mastic gum essential oil and detection of adulteration in mastic oil products with the application of chiral and non-chiral GC-MS analysis, Fitoterapia 114 (2016) 12–17.
[26] S.H. Cho, H.J. Park, J.H. Lee, J.A. Do, S. Heo, J.H. Jo, S. Cho, Determination of anabolic-androgenic steroid adulterants in counterfeit drugs by UHPLC-MS/MS, J. Pharm. Biomed. Anal. 111 (2015) 138–146.
[27] J. Fiori, V. Andrisano, LC-MS method for the simultaneous determination of six glucocorticoids in pharmaceutical formulations and counterfeit cosmetic products, J. Pharm. Biomed. Anal. 91 (2014) 185–192.
[28] G. Pagliuca, C. Bozzi, F.R. Gallo, G. Multari, G. Palazzino, R. Porra, A. Panusa, Triacylglycerol "hand-shape profile" of Argan oil. Rapid and simple UHPLC-PDA-ESI-TOF/MS and HPTLC methods to detect counterfeit Argan oil and Argan-oil-based products, J. Pharm. Biomed. Anal. 150 (2018) 121–131.
[29] S. Orecchio, R. Indelicato, S. Barreca, Determination of selected phthalates by gas chromatography-mass spectrometry in personal perfumes, J. Toxicol. Environ. Health 78 (15) (2015) 1008–1018.
[30] Y. Aghoutane, M. Brebu, M. Moufid, R. Ionescu, B. Bouchikhi, N. El Bari, Detection of counterfeit perfumes by using GC-MS technique and electronic nose system combined with chemometric tools, Micromachines 14 (3) (2023) 524.
[31] B. Pacholczyk-Sienicka, G. Ciepielowski, L. Albrecht, The first application of H-1 NMR spectroscopy for the assessment of the authenticity of perfumes, Molecules 26 (11) (2021) 3098.
[32] M. Zangheri, M.M. Calabretta, D. Calabria, J. Fiori, M. Guardigli, E. Michelini, S. Melandri, A. Maris, M. Mirasoli, L. Evangelisti, Immunological analytical techniques for cosmetics quality control and process monitoring, Processes 9 (11) (2021) 1982.
[33] L. Bu, S. Li, L. Nie, L. Jiang, G. Dong, D. Song, Q. Zhou, Construction of fluorescent sensor array with nitrogen-doped carbon dots for sensing Sudan Orange G and identification of various azo compounds, J. Colloid Interface Sci. 663 (2024) 403–413.
[34] T. Wang, X. Yang, J. Men, J. Zhou, H. Zhang, A near-infrared fluorescent probe based on boric acid hydrolysis for hydrogen peroxide detection and imaging in HeLa cells, Luminescence 35 (2) (2020) 208–214.
[35] H.T. Zhang, R.C. Liu, Y. Tan, W.H. Xie, H.P. Lei, H.Y. Cheung, H.Y. Sun, A FRET-based ratiometric fluorescent probe for nitroxyl detection in living cells, ACS Appl. Mater. Interfaces 7 (9) (2015) 5438–5443.
[36] .
[37] Z.H. Mohamed, C. Rhein, B. Schmid, P. Tripal, J. Kornhuber, C. Arenz, Synthesis and characterization of a new two photon excitable acid sphingomyelinase FRET probe, Biorg. Med. Chem. 44 (2021) 116303.
[38] Z.H. Mohamed, C. Rhein, E.M. Saied, J. Kornhuber, C. Arenz, FRET probes for measuring sphingolipid metabolizing enzyme activity, Chem. Phys. Lipids 216 (2018) 152–161.
[39] C.E. Rowland, C.W. Brown, I.L. Medintz, J.B. Delehanty, Intracellular FRET-based probes: a review, Methods Appl. Fluoresc. 3 (4) (2015) 042006.
[40] A. Auer, M.T. Strauss, T. Schlichthaerle, R. Jungmann, Fast, background-free DNA-PAINT imaging using FRET-based probes, Nano Lett. 17 (10) (2017) 6428–6434.
[41] K. Quan, C.P. Yi, X.H. Yang, X.X. He, J. Huang, K.M. Wang, FRET-based nucleic acid probes: basic designs and applications in bioimaging, Trac. Trends Anal. Chem. (2020) 115784.
[42] K. Kiyose, S. Aizawa, E. Sasaki, H. Kojima, K. Hanaoka, T. Terai, Y. Urano, T. Nagano, Molecular design strategies for near-infrared ratiometric fluorescent probes based on the unique spectral properties of aminocyanines, Chemistry 15 (36) (2009) 9191–9200.
[43] F. Rispo, G. De Negri Atanasio, I. Demori, G. Costa, E. Marchese, S. Perera-del-Rosario, E. Serrano-Candelas, M. Palomino-Schätzlein, E. Perata, F. Robino, An extensive review on phenolic compounds and their potential estrogenic properties on skin physiology, Front. Cell Dev. Biol. 11 (2024) 1305835.
[44] M.Á. Moro, V.M. Darley-Usmar, I. Lizasoain, Y. Su, R.G. Knowles, S. Moncada, M. W. Radomski, The formation of nitric oxide donors from peroxynitrite, Br. J. Pharmacol. 116 (3) (1995) 1999–2004.